Ocean Waves Measurement and Analysis, Fifth International Symposium WAVES 2005, 3rd-7th, July, 2005. Madrid, Spain
Paper number: 197

WAVE ENERGY FOCUSING IN A THREE-DIMENSIONAL NUMERICAL WAVE TANK

Stéphan T. Grilli, M.ASCE [1], Christophe Fochesato [2] and Frédéric Dias [3]

Abstract: Extreme waves at sea, so-called freak waves, are simulated in a three-dimensional (3D) fully nonlinear Numerical Wave Tank (NWT), through wave energy focusing achie- ved from the motion of a snake wavemaker. Wave kinematics is analysed near the crest from the numerical simulations. By contrast with simple linear superposition, nonlinear interactions enhance energy focusing and generate larger more damaging waves. The NWT solves incompressible free-surface Euler equations for potential flows, with a higher-order Boundary Element Method and a mixed Eulerian-Lagrangian time updating. The numerical efficiency of the NWT was recently improved by the implementation of the Fast Multipole Algorithm in the spatial solver. A typical case of an overturning, near breaking, rogue wave is presented as an application. Detailed wave shapes are given, as well as results for the particle velocities at the surface and under the wave crest.

INTRODUCTION

This study deals with the rare but important phenomenon of freak waves at sea. Despite their low probability of occurrence, such waves may cause severe damages to ocean structures located in their path. Hence, dynamic loads caused by freak waves must be considered when design important off-shore or naval structures. Freak waves are localized in time and space and result from a short duration local focusing of wave energy, which may be due to a number of factors. Among these, spatial wave energy focusing is one of the most commonly proposed mechanisms to explain the appearance of rogue waves. According to linearized wave theory, wave components with different phases and directions can superimpose over a small region of space and time to produce a much larger wave. Such superposition is enhanced by nonlinear effects (e.g., Grilli and Brandini, 2001). Other factors, however, may cause wave energy focusing, such as the bottom topography in shallow water, or wave-current interactions. In deep water, the 'Benjamin-Feir' modulational instability may cause self-focusing of wave energy (e.g., Henderson *et al.*, 1999). Other wave-wave interactions or interactions with atmospheric conditions may also play a role in this phenomenon. Kharif and Pelinovsky (2003) summarized these mechanisms in their recent review article.

[1]Distinguished Professor and Chair at the University of Rhode Island, Depart. of Ocean Engng., Narragansett, RI 02882, grilli@oce.uri.edu.

[2]Université de Bordeaux, Talence, France, Christophe.Fochesato@math.u-bordeaux1.fr.

[3]Professor and Chair, ENS de Cachan, 61, av. Président Wilson, F94235 Cachan, France, Frederic.Dias@cmla.ens-cachan.fr

While most studies of rogue waves so far have assumed deep water, it has been shown that these waves can occur for any water depth. Here, we consider an arbitrary finite depth, but specify a flat bottom in order to concentrate on one focusing mechanism only. Our model can however feature an arbitrary bottom topography.

Early two-dimensional (2D) studies, both numerical and experimental, used the mechanism of frequency focusing, which occurs when faster waves catch slower ones that have been generated earlier, to create wave superposition (Chaplin, 1996). More recently, spatial energy focusing has been the typical mechanism used to generate extreme waves in three-dimensional (3D) laboratory wave tank. To do so, a properly programmed snake wavemaker creates the superposition of several directional sinusoidal wave components. She *et al.* (1994), for instance, made such laboratory experiments and studied the kinematics of breaking waves using a PIV technique. Brandini and Grilli (2001) and Brandini (2001) carried out a 3D numerical study of spatial wave focusing with the Boundary Element model of Grilli *et al.* (2001), by implementing both a snake wavemaker to generate waves at one extremity of a 3D NWT, and an open absorbing boundary at the other extremity. More recently, Bonnefoy *et al.* (2004) developed a NWT based on a higher-order spectral solution of Euler's equations with a free surface, and compared their results with experiments. Although their method cannot model overturning waves, it allows to consider many wave components in a large basin, and thus to generate realistic random wave fields.

By contrast, the goal of the present study is to numerically simulate intense directional energy focusing in a 3D-NWT, leading to wave overturning, and study the kinematics of such extreme waves near the crest. Following Grilli and Brandini (2001), we use a Boundary Element Method (BEM) to solve Euler equations with a free surface. The computational cost of the original method, however, which grows quadratically with the discretization, makes such computations rapidly prohibitive. We eliminate this obstacle by implementing the Fast Multipole Algorithm (FMA) to accelerate all the matrix-vector products in the spatial solver (Fochesato and Dias, 2004), and achieve a computational cost almost proportional to the discretization size, i.e., O(N). Greengard and Rokhlin (1987) initially developed the FMA for the N-body problem, and allow for a faster computation of all pair-wise interactions. The FMA, in particular, is well suited to compute interactions governed by Laplace's equation and, hence, for our problem. The FMA takes advantage of the fact that the strength of pair-wise interactions decreases with distance, so that far distant points can be regrouped together, to contribute to one collocation point. A hierarchical subdivision of space automatically provides distance criteria to separate close interactions from distant ones. The FMA can be used to directly solve Laplace's equation, but it can also be associated with an integral representation of Laplace's equation, such as the BEM, which leads to a linear discretized system of equations, with matrix-vector products. The solution of this system with an iterative solver can be greatly accelerated by the FMA. Rokhlin (1985) applied this idea to the equations of potential theory. [See the review article by Nishimura (2002) on the application of this algorithm for boundary integral equation methods.]

Korsmeyer et al. (1993) already combined the FMA with a BEM, using a Krylov-subspace iterative algorithm. Following Rokhlin's ideas, they designed a modified FMA for the equations of potential theory. Initially developed for electrostatic analyses, their code was generalized to become a fast Laplace solver, which subsequently was used for potential fluid flows. Theirs was an efficient model but its global accuracy was limited due to the use

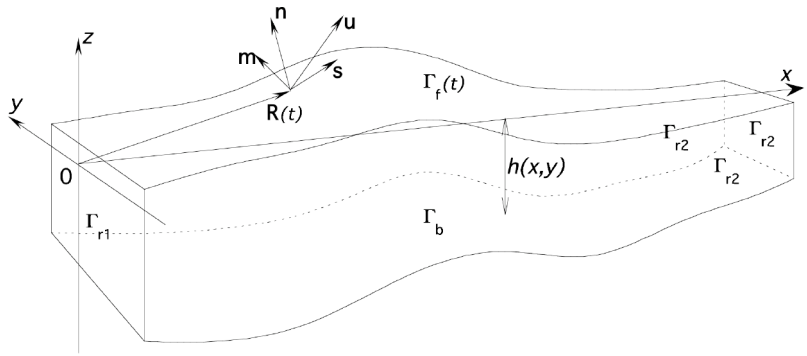

Fig. 1. Sketch of computational domain for 3D-NWT.

of low order BEM elements. Scorpio and Beck (1996) studied wave forces on bodies with a multipole-accelerated desingularized method, and thus did not use a BEM to discretize the problem. Neither did Graziani and Landrini (1999), who used the Euler-McLaurin quadrature formula in their 2D model. For completion, let us just point out that other fast methods exist for water waves, essentially spectral methods based on the Fast Fourier Transform. In particular, the recent work by Bonnefoy et al. (2004), cited above, is a NWT for non-breaking waves, that uses a spectral method and also has a O(N) numerical complexity.

In the following, we show how the FMA can be combined with the NWT by Grilli et al. (2001) to yield a much more efficient numerical tool. The modified model is then applied to freak wave generation, over much more refined discretizations than could be used in the past. Thus, physical processes can be better represented and analyzed in these new simulations. Details of the FMA can be found in Fochesato and Dias (2004). The next section presents the numerical model and its more recent improvements. Then the configuration of the NWT used for freak wave simulations is described. Finally, results are presented and discussed for one application.

BACKGROUND OF NUMERICAL MODEL

The basic formalism is that of Grilli et al.'s (2001) NWT. We consider the equations for a potential flow of an ideal, incompressible fluid, with a free surface. Within the domain, the governing equation is Laplace's equation, $\Delta\phi = 0$ for the velocity potential ϕ, defined from the velocity as, $\boldsymbol{u} = \boldsymbol{\nabla}\phi$. Green's second identity transforms this equation into a Boundary Integral Equation (BIE),

$$\alpha(\boldsymbol{x}_l)\,\phi(\boldsymbol{x}_l) = \int_{\Gamma(t)} \left\{ \frac{\partial\phi}{\partial n}(\boldsymbol{x})\, G(\boldsymbol{x},\boldsymbol{x}_l) - \phi(\boldsymbol{x})\, \frac{\partial G}{\partial n}(\boldsymbol{x},\boldsymbol{x}_l) \right\} \mathrm{d}\Gamma \tag{1}$$

where $G(\boldsymbol{x},\boldsymbol{x}_l) = \frac{1}{4\pi\, d}$ is the 3D free space Green's function, $d = |\boldsymbol{x} - \boldsymbol{x}_l|$, $\boldsymbol{n}$ is the normal vector exterior to the boundary and $\alpha(\boldsymbol{x}_l)$ is proportional to the exterior solid angle of the boundary at collocation point $\boldsymbol{x}_l$ (Fig. 1). On the free surface, the potential ϕ satisfies the nonlinear kinematic and dynamic boundary conditions,

$$\frac{D\,\boldsymbol{R}}{D\,t} = \boldsymbol{\nabla}\phi \quad ; \quad \frac{D\,\phi}{D\,t} = -gz + \frac{1}{2}\,\boldsymbol{\nabla}\phi\cdot\boldsymbol{\nabla}\phi \tag{2}$$

respectively, where $\boldsymbol{R}$ is the position vector of a fluid particle on the free surface, g the acceleration due to gravity and D/Dt the material derivative. Lateral boundaries are either

fixed or moving boundaries. In this study, waves are generated by a snake flap wavemaker, at the open boundary $\Gamma_{r1}(t)$. The motion $\boldsymbol{x}_p$ and velocity $\boldsymbol{u}_p$ of the wavemaker are specified as, $\overline{\boldsymbol{x}} = \boldsymbol{x}_p$ and $\overline{\frac{\partial \phi}{\partial n}} = \boldsymbol{u}_p \cdot \boldsymbol{n}$, where overlines denote specified values. Along the fixed parts of the boundary, such as the bottom Γ_b and lateral boundaries Γ_{r2}, a no-flow condition is prescribed as, $\overline{\frac{\partial \phi}{\partial n}} = 0$.

Flow kinematics can be explicitly calculated inside the domain based on the boundary solution of Eq. (1). For instance, velocity and local acceleration at internal point $\boldsymbol{x}_l$ are given by,

$$\begin{aligned} \boldsymbol{u}_l = \boldsymbol{\nabla}_l \, \phi(\boldsymbol{x}_l) &= \int_{\Gamma(t)} \left\{ \frac{\partial \phi}{\partial n}(\boldsymbol{x}) \, Q(\boldsymbol{x}, \boldsymbol{x}_l) - \phi(\boldsymbol{x}) \, \frac{\partial Q}{\partial n}(\boldsymbol{x}, \boldsymbol{x}_l) \right\} \mathrm{d}\Gamma \\ \frac{\partial \boldsymbol{u}_l}{\partial t} = \boldsymbol{\nabla}_l \, \frac{\partial \phi}{\partial t}(\boldsymbol{x}_l) &= \int_{\Gamma(t)} \left\{ \frac{\partial^2 \phi}{\partial t \partial n}(\boldsymbol{x}) \, Q(\boldsymbol{x}, \boldsymbol{x}_l) - \frac{\partial \phi}{\partial t}(\boldsymbol{x}) \, \frac{\partial Q}{\partial n}(\boldsymbol{x}, \boldsymbol{x}_l) \right\} \mathrm{d}\Gamma \end{aligned} \qquad (3)$$

respectively, where $Q(\boldsymbol{x}, \boldsymbol{x}_l) = \frac{1}{4\pi d^3} \boldsymbol{d}$, $\frac{\partial Q}{\partial n}(\boldsymbol{x}, \boldsymbol{x}_l) = \frac{1}{4\pi d^3} \{ \boldsymbol{n} - 3(\boldsymbol{e}_d \cdot \boldsymbol{n}) \boldsymbol{e}_d \}$, with $\boldsymbol{e}_d = \frac{1}{d} \boldsymbol{d}$ and $\boldsymbol{\nabla}_l$ the gradient operator with respect to internal point $\boldsymbol{x}_l$.

The domain shown in Fig. 1 represents a closed basin such as a wave tank, whose bottom can be defined with arbitrary geometry. The numerical model is presented in detail in Grilli *et al.* (2001) and Fochesato et al. (2005). The time stepping algorithm consists in updating the position vector and the velocity potential on the free surface, based on second-order Taylor series expansions. At each time step, The BIE (1) is solved through the use of a Boundary Element Method (BEM). The boundary is divided into elements for which a local interpolation is defined, both for the geometry and field variables. Bi-cubic polynomial shape functions are used and a local change of variables is defined to express BIE integrals on a curvilinear reference element. The numerical computation of these integrals is performed using a Gauss-Legendre quadrature and appropriate techniques are applied for removing weak singularities of the Green's functions. The number of discretization nodes yields the assembling phase of the discretization matrix. The latter is modified by applying the rigid mode technique, which allows to directly compute the solid angles α and thus avoid evaluating the strongly singular integrals of the normal derivative of the Green's function. The use of the multiple node technique, to deal with domain edges and corners also leads to a modification of the algebraic system matrix. The velocity potential, or its normal derivative depending on the boundary condition, is obtained by solving the resulting linear system of equation. Since the system matrix is fully populated and non-symmetric, the method has at best a N^2 computational complexity, where N is the number of nodes in the discretization, when using the iterative algorithm GMRES (optimized conjugate gradient method). Thus the spatial solution at each time step is of the same complexity as the assembling of the system matrix. The FMA is implemented to reduce this complexity and increase the solution efficiency when evaluating every matrix-vector in the discretization of the BIE.

The FMA is based on the principle that the Green's function can be expanded in separated variables (i.e., spherical harmonics) when the source point $\boldsymbol{x}_l$ and the evaluation point $\boldsymbol{x}$ are far enough from each other on the boundary. Thus, one can write for a point O (origin of the

expansion) close to $\boldsymbol{x}$ and far from $\boldsymbol{x}_l$,

$$G(\boldsymbol{x},\boldsymbol{x}_l) \approx \frac{1}{4\pi}\sum_{k=0}^{p}\sum_{m=-k}^{k}\rho^k Y_k^{-m}(\alpha,\beta)\frac{Y_k^m(\theta,\varphi)}{r^{k+1}} \tag{4}$$

where $O\boldsymbol{x} = (\rho,\alpha,\beta)$ and $O\boldsymbol{x}_l = (r,\theta,\varphi)$ in spherical coordinates. Functions $Y_k^{\pm m}$ are the spherical harmonics defined from Legendre polynomials. In order to determine in which cases this approximation can be used, a spatial hierarchical subdivision of the domain is defined based on distance criteria. Close interactions are evaluated with standard Green's functions and far interactions are approximated based on the subdivision into cells and expansions of the Green' functions with Eq. (4). Error and complexity analyses for the FMA are given for instance by Greengard (1988). In our case, the FMA must be adapted in order to be part of our wave model. Thus, the integral Eq. (1) can be written as,

$$\alpha(\boldsymbol{x}_l)\,\phi(\boldsymbol{x}_l) \approx \frac{1}{4\pi}\sum_{k=0}^{p}\sum_{m=-k}^{k} M_k^m(O)\frac{Y_k^m(\theta,\varphi)}{r^{k+1}} \tag{5}$$

where $M_k^m(O)$ is the moment at the origin O,

$$M_k^m(O) = \int_\Gamma \left\{ \frac{\partial\phi}{\partial n}(\boldsymbol{x})\,\rho^k\,Y_k^{-m}(\alpha,\beta) - \phi(\boldsymbol{x})\,\frac{\partial}{\partial n}\left(\rho^k\,Y_k^{-m}(\alpha,\beta)\right)\right\} \mathrm{d}\Gamma \tag{6}$$

Based on Eqs. (5),(6), we now consider the contribution of boundary element to a collocation point. The local computation of several elements grouped together into a multipole relies on a BEM analysis, using the spherical harmonics instead of the Green's function. The integration of the normal derivative of the spherical harmonics is done by taking care of avoiding an apparent singularity, which could generate numerical errors. The BEM discretization only takes place in the computation of the moments. The rest of the FMA is standard, especially the translation and conversion formulae, which allow to pass information through the hierarchical spatial subdivision, from the multipole contributions to the evaluation at every collocation point. From the wave model point of view, we had to adapt all the aspects depending on the existence of the system matrix in the former BEM model.

The accelerated FMA model benefits from the faster Laplace's equation solver at each time step. The FMA model performance was tested by comparing new results with the former model's results for a 3D application, which requires great accuracy : the propagation of a solitary wave on a sloping bottom with a transverse modulation, leading to a plunging jet (Grilli et al., 2001). The consistency of the new approximation was checked but, more importantly, the accuracy and stability of results and their convergence with the discretization size was verified. In fact, by adjusting the parameters of the FMA, i.e., the hierarchical spatial subdivision and the number of terms p in the multipole expansions, one can get the same numerical results as with the former model. In this application, for discretizations having more than $N = 4,000$ nodes, the computational time was observed to evolve nearly linearly with N. See Fochesato and Dias (2004) for detail.

NWT FOR 3D ENERGY FOCUSING

Here, the NWT is defined as a rectangular basin with a flat bottom of depth h_0. A snake wavemaker is implemented at one extremity (Grilli and Brandini, 2001), as a series of flap

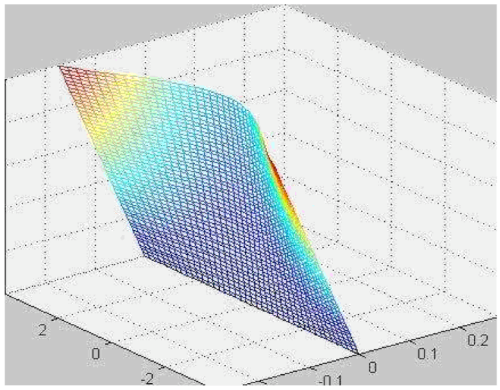

Fig. 2. Typical snake wavemaker motion on the leftward extremity of the NWT.

paddles rotating on the bottom with the angular velocity $\dot{\Omega}\,\boldsymbol{j}$. Each paddle position is defined as, $\boldsymbol{x}_p = (x_p, y_p, z_p) = \boldsymbol{x}_o - \rho\,\boldsymbol{m}$, with $\boldsymbol{x}_o = y_p\,\boldsymbol{j} - h_o\,\boldsymbol{k}$, the coordinates of the axis of rotation and ρ the distance from the axis of rotation, measured on the paddle in the vertical plane. Hence,

$$\rho = \sqrt{x_p^2 + (h_o + z_p)^2} \quad \text{, and} \quad \Omega = \arctan\left\{\frac{S_o}{h_o}\right\} \tag{7}$$

where $S_o(y,t)$ is the horizontal paddle stroke specified at $z = 0$. From these definitions, we find the velocity and acceleration vectors on the wavemaker as,

$$\boldsymbol{u}_p = -\dot{\rho}\,\boldsymbol{m} - \rho\,\dot{\Omega}\,\boldsymbol{n} \quad ; \quad \frac{\mathrm{d}\boldsymbol{u}_p}{\mathrm{d}t} = \left\{\rho\,\dot{\Omega}^2 - \ddot{\rho}\right\}\boldsymbol{m} - \left\{2\,\dot{\rho}\,\dot{\Omega} + \rho\,\ddot{\Omega}\right\}\boldsymbol{n} \tag{8}$$

Following Dalrymple (1989), we specify the wavemaker stroke S_o as the linear superposition of N_θ sinusoidal components of amplitude a_n and direction θ_n, as

$$S_o(y,t) = \sum_{n=1}^{N_\theta} a_n \cos\left\{k_n(y\sin\theta_n - x_f\cos\theta_n) - \omega_n t\right\} \tag{9}$$

where k_n and ω_n denote the wavenumber and circular frequency of each component, respectively, which are related by the linear dispersion relationship, $\omega_n^2 = g\,k_n\,\tanh(k_n h_o)$, and x_f is the focusing distance for the waves in front of the wavemaker. Angles θ_n are uniformly distributed in the range $[-\theta_{\max}, \theta_{\max}]$. Only directional focusing is studied here, hence $\omega_n = \omega$. [Frequency focusing could be specified by adjusting the components' frequency as a function of the angle θ_n.] Moreover, for simplicity, we use identical component amplitudes; different values however could as easily be selected.

The first objective of this work has consisted in finding wavemaker parameter values such that an extreme overturning wave is generated near the middle of the NWT. The variables are non-dimensionalized (length by depth h_0, and time by $\sqrt{h_0/g}$). The NWT is 10 unit long along the x axis and 20 units wide along the y axis. We consider the superposition of $N_\theta = 10$ components having identical amplitude $a_n = 0.035$, and directions θ_n varying between -45 and 45 degrees. Every component has a frequency $\omega_n = 1.2816$, which gives a linear wavelength $L = 2\pi/k = 3.725$, velocity $c = \omega/k = 0.7599$, and steepness $ka = 0.059$. The energy focusing point is specified at the distance $x_f = 7.5$ from the wavemaker. At the beginning of the computations, the BEM discretization uses 60 elements in

the x direction, which corresponds to roughly 20 nodes per wavelength. In order to obtain the overturning phase, this resolution is improved to 75 elements from $t \approx 16.25$. The width of the domain is divided into 70 elements, and the depth into 4 elements. [Note that all the boundaries are discretized in the present simulations, unlike in Brandini and Grilli's (2001) work, that used an image method to eliminate the bottom discretization; this simplification will be implemented in the FMA, in future work.] Fig. 2 shows a typical motion of the snake wavemaker in the NWT. At the other extremity of the domain, an absorbing piston boundary is specified (Clément, 1996; Grilli and Horrillo, 1997; Grilli and Brandini, 2001), although it is not perfectly suited to these intermediate depth waves. Nevertheless, this condition sufficiently delays the instant when reflection can no longer be neglected in computations, to allow us to study the extreme 3D overturning wave generated in the NWT. [The implementation of an absorbing piston having the same kind of movement as the snake wavemaker, as in Brandini and Grilli (2001), would improve this feature.]

APPLICATIONS

Figure 3 presents the time evolution of the free surface computed in the NWT, using the wavemaker parameters and BEM discretization discussed in the previous section. To reduce the initial singularities at the interface between the free surface and the moving boundary, the wavemaker motion was ramped up over three periods (Grilli and Brandini, 2001). The initially flat and still free surface starts moving near the wavemaker, and a first focused wave of moderate amplitude is generated (Figs. 3a,b). Then, the wave elevation decreases, before disappearing. Hence, we effectively model some local wave focusing, which is transient both in time and space, a known characteristic of freak waves. Behind this first wave, a second wave appears, which clearly results from the superposition of wave components with different directions (Figs. 3c). The amplitude of the wavemaker oscillations increases further and the sum of the wave components gives rise to an even larger wave in the middle of the tank. This wave steepens while approaching the focal point, theoretically specified at $x = 7.5$. Wave overturning is initiated when the crest is located at $x = 4.0$ (Fig. 3d). Behind the latter wave, the phenomenon is starting to repeat itself, with a new curved crest line appearing and converging towards the focal point.

A closer analysis of the computed free surface shapes leads to the following comments. The largest focused wave appears like a curved front, with maximum elevation significantly larger than that of the following waves, which have not yet converged. A circular trough is created just in front of the focused wave (the so-called "hole in the sea" reported by freak wave eyewitnesses), and an even deeper, crescent shape, trough forms behind it, separating the main wave from the curved crest line following it. There is a strong asymmetry between the focused wave front and its back. This asymmetry increases with time and indicates that the wave is about to break. In the present case where the directionality is important, the front is not so wide, and 3D effects are emphasized (note, axes sclaes are distorted in the figures). The properties of this extreme wave, generated in the NWT, thus qualitatively agree with observed geometrical properties of freak waves. In particular, Fig. 4 (left) shows a vertical cross-section of the solution obtained at $y = 0$ and $t = 18.05$. We see, the wave profile is similar to that observed in many actual freak wave measurements, as well as computed in earlier 2D numerical studies of modulational instabilities of a wave packet (e.g., Kharif and Pelinovski, 2003): the wave crest amplitude is much larger than the trough amplitudes and the back trough is deeper than the front one. The crest peaks at $z = 0.38$, and the back and

front troughs are respectively measured at $z = -0.17$ and $z = -0.10$. It is remarkable that we get such a 2D characteristic shape, whereas the mechanism of wave generation used here is purely 3D. This suggests some independence of freak wave shapes and properties from the phenomena that have generated it. Fig. 4 (right) shows a profile of the solution at the final computed time $t = 18.36$, when the wave is overturning.

Velocity and acceleration fields computed on the free surface (see Guyenne and Grilli, 2003, for detail) show two main phases in the evolution of this focused wave event. The first phase is one of approach, where the different wave components forming a crest line are converging towards the focal point. The obtained kinematics simply corresponds to the propagation of a curved crest line. The second phase corresponds to the appearance of a single focused wave, resulting from the directional superposition of many components. The maximum value of the longitudinal velocity component increases and the largest velocities concentrate more and more at the focused wave crest, indicating flow convergence. As a result, this crest tends to go forward faster than its basic wave components, thus initiating wave overturning. At the same time, the transverse component of the velocity and acceleration fields show that 3D effects are reduced near the wave front face. Hence, the dynamics of imminent breaking of the freak wave takes an almost 2D configuration. [This observation has important implications for the design of offshore structures that would be located in the path of such a wave.] This is in good agreement with some description of a "wall of water", that we can find in stories about extreme wave events in the ocean. Examples of results for the wave kinematics at some internal points, in a vertical cross-section at $y = 0$ under the wave crest, and in the plunging jet are given in Fig. 5. The maximum velocity in the crest is $1.1\sqrt{gh_0}$ during overturning.

CONCLUSIONS

We gave an overview of a 3D-NWT simulating directional wave energy focusing, based on a BEM solution of potential flow equations. Recent model improvements were presented, in particular, the use of the FMA, which has a $O(N)$ numerical complexity. In the single application presented, we generated an extreme wave event, using a snake wavemaker. Properties of the generated extreme waves are briefly discussed (shape and kinematics). Brandini and Grilli (2001) presented a similar study based on an earlier version of this NWT. They could not however, reach the overturning phase for an extreme wave event, both due to limitations in the model implementation (now corrected; see Fochesato et al., 2005) and discretization size that could be realistically used. Here, we observe, a vertical 2D slice through the extreme wave crest is quite similar to the characteristic shape measured for freak waves in the ocean. The 3D wave generation yields a curved wave front, before focusing occurs, with a circular trough in front of the wave, followed by a deeper trough with a crescent shape. The kinematics shows two main phases: (i) a converging curved crest; (ii) a steepening wave with velocity and acceleration vectors on the front face having weak transverse components. After focusing, wave overturning seems essentially similar to 2D wave dynamics. This corresponds to the reported aspect of a "wall of water" in the ocean. More details will be given during the conference.

REFERENCES

Broeze J. (1993). "Numerical modelling of nonlinear free surface waves with a three-dimensional panel method." *PhD thesis, University of Twente, Enschede, The Netherlands.*

Bonnefoy F., Le Touze D., and Ferrant P. (2004). "Generation of fully-nonlinear prescribed wave fields using a high-order spectral method," *Proc. 14th Offshore and Polar Engng. Conf.* (ISOPE 2004), Toulon, France, vol. III, 257–263.

Brandini C. (2001). *Nonlinear interaction processes in extreme wave dynamics,* Ph.D. Dissertation, University of Firenze.

Brandini C. and Grilli S. (2001). "Modeling of freak wave generation in a 3D-NWT," *Proc. 11th Offshore and Polar Engng. Conf.* (ISOPE 2001), Stavanger, Norway, Vol III, 124–131.

Chaplin, J.R. (1996). "On frequency-focusing unidirectional waves," *Intl. J. Offshore and Polar Engng.*, **6**, 131–137.

Clément A. (1996). "Coupling of two absorbing boundary conditions for 2D time-domain simulations of free surface gravity waves," *J. Comp. Phys.*, **26**, 139–151.

Dalrymple R.A. (1989). "Directional wavemaker theory with sidewall reflection," *J. Hydraulic Res.*, **27** (1), 23–34.

Fochesato C. and Dias F. (2004). "Numerical model using the Fast Multipole Algorithm for nonlinear three-dimensional free-surface waves," (preprint CMLA).

Fochesato, C., Grilli, S. and Guyenne P. (2005). "Note on non-orthogonality of local curvilinear coordinates in a three-dimensional boundary element method," *Intl. J. Numer. Meth. In Fluids* (in press).

Graziani G., Landrini M. (1999). "Application of Multipoles Expansion Technique to Two-Dimensional Nonlinear Free-Surface Flows," *J. Ship Research.* **43**, 1–12.

Greengard L. (1988). *The Rapid Evaluation of Potential Fields in Particle Systems,* MIT Press, Cambridge, MA.

Greengard L., Rokhlin V. (1987). "A fast algorithm for particle simulations," *J. Comput. Phys.* **73**, 325–348.

Grilli S., Guyenne P., and Dias F. (2001). "A fully nonlinear model for three-dimensional overturning waves over arbitrary bottom," *Int. J. Num. Meth. Fluids*, **35**, 829–867.

Grilli S.T. and Horrillo J. (1997). "Numerical Generation and Absorption of Fully Nonlinear Periodic Waves," *J. Engng. Mech.*, **123** (10), 1060–1069.

Guyenne, P. and Grilli, S.T. (2003). "Numerical study of three-dimensional overturning waves in shallow water", *J. Fluid Mech.* (in revision).

Henderson, K.L., Peregrine, D.H. and Dold, J.W. (1999). "Unsteady water wave modulations: fully non linear solutions and comparison with the non linear Schrödinger equation," *Wave motion*, **9**, 341–361.

Kharif C. and Pelinovsky E. (2003). "Physical mechanisms of the rogue wave phenomenon," *Eur. J. Mech. B-Fluids*, **22** (6), 603–634.

Korsmeyer F.T., Yue D.K.P. and Nabors K. (1993). "Multipole-Accelerated Preconditioned Iterative Methods for Three-Dimensional Potential Problems," presented at *BEM 15*, Worcester, MA.

Nishimura, N. (2002). "Fast multipole accelerated boundary integral equation methods," *Appl. Mech. Rev.* **55**, 299–324.

Rokhlin V. (1985). "Rapid solution of integral equations of classical potential theory," *J. Comput. Phys.* **60**, 187–207.

Scorpio S., Beck F. (1996). "A Multipole Accelerated Desingularized Method for Computing Nonlinear Wave Forces on Bodies," *15th Intl. Conf. Offsh. Mech. Arctic Engng.*, Florence, Italy.

She K., Greated C.A., and Easson W.J. (1994). "Experimental study of three-dimensional wave breaking," *J. Waterway, Port, Coastal and Ocean Engng.*, **120**, 20–36.

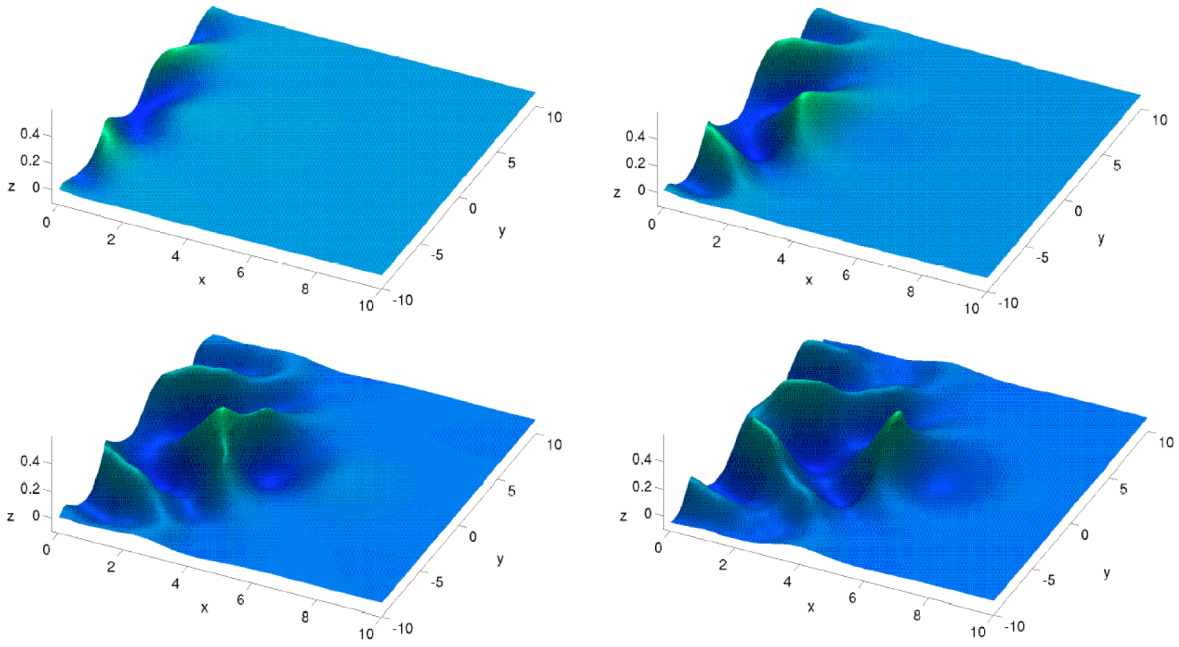

Fig. 3. Free surface evolution : (a) at $t = 6.36$, (b) at $t = 10.96$, (c) at $t = 16.25$, (d) at $t = 18.36$.

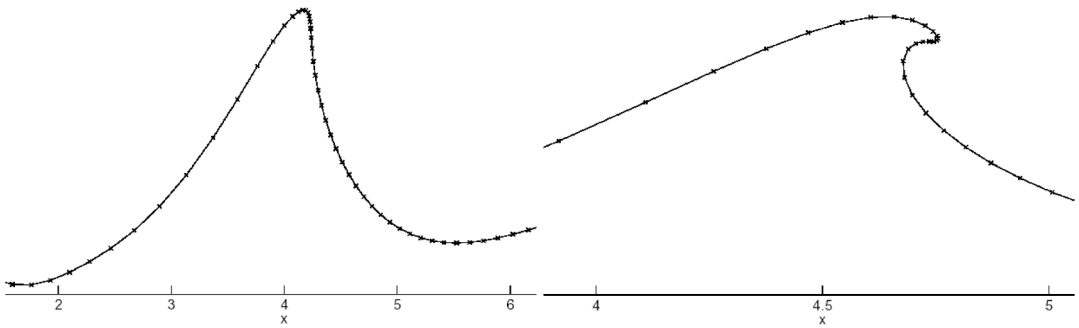

Fig. 4. Free surface at $y = 0$: $t = 17.84$ (left) and $t = 18.36$ (right).

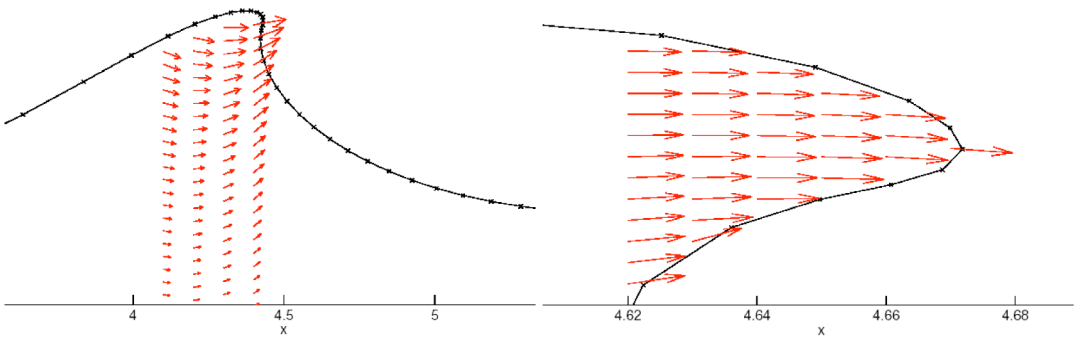

Fig. 5. Free surface and velocity at $y = 0$: $t = 18.05$ (left) and $t = 18.28$ (right).